8.4 MIGFA: THE MACHINE INTELLIGENT GUST FRONT ALGORITHM FOR NEXRAD

David J. Smalley*
Betty J. Bennett
Robert Frankel
MIT Lincoln Laboratory, Lexington, Massachusetts

1. INTRODUCTION†

Over a decade ago the FAA identified a need to detect and forecast movement of wind shear hazards such as gust fronts that impact the terminal air space. The Machine Intelligent Gust Front Algorithm (MIGFA) was developed to address this need (Delanoy and Troxel, 1993). The MIGFA product provides the position, the forecasted positions, and the strength of each wind shear detection to support air traffic control safety and planning functions.

MIGFA will realize a new capability for NEXRAD but was originated for use with the FAA's Airport Surveillance Radar Model 9 (ASR-9) Weather Systems Processor (WSP) as described in Troxel and Pughe (2002). Subsequently, a second version was developed for the FAA's Terminal Doppler Weather Radar (TDWR) and is a component of the FAA's Integrated Terminal Weather System (ITWS). Most of the larger U.S. airports have ITWS installations. The ASR-9s are associated with medium-sized airports. MIGFA in NEXRAD is intended to further expand MIGFA support of air traffic control functions.

There are significant algorithmic differences between the ASR-9 WSP and TDWR versions of MIGFA, primarily because of the different beam types of the two radars. Physically, the TDWR's pencil beam allows for good vertical resolution in a spatial volume of data. The ASR-9's vertical fan beam results in poor vertical resolution. Nonetheless, a key tenet in developing these two versions of MIGFA was to use the same core image processing analysis techniques (Morgan and Troxel, 2002) central to the MIGFA functionality. This same core is also central to MIGFA in NEXRAD.

The Massachusetts Institute of Technology's Lincoln Laboratory (LL) has been tasked by the FAA to transfer MIGFA technology to NEXRAD. The goal is to enable a NEXRAD MIGFA capability at airports within about 70 km of any NEXRAD. LL has been developing NEXRAD algorithms to address the FAA's weather systems' needs since the Open Radar Product Generator (ORPG) was fielded in 2001. FAA sponsored, LL-developed NEXRAD algorithms generate the following products: the Data Quality Assurance (DQA), the High Resolution VIL (HRVIL), and the High Resolution Enhanced Echo Tops (HREET) (Smalley *et al.*, 2003). These algorithms have proven useful to non-FAA users of NEXRAD products such as the National Weather Service (NWS) and the Department of Defense (DoD). Similarly, the NWS and DoD are developing plans to use MIGFA. MIGFA is slated to be included in the ORPG Build 9 baseline that is scheduled to be released in the Spring of 2007.

In the following sections, we will discuss the salient features of MIGFA; the tuning of MIGFA to NEXRAD data; a comparison of detection performance of the

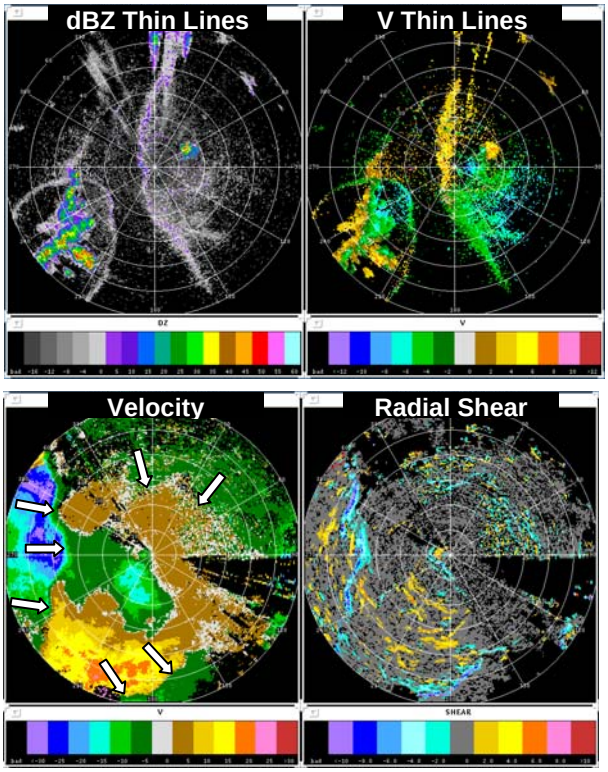

Figure 1. MIGFA relies on image processing of basic radar data to generate interest fields relating to various aspects of the data. Important features of note are thin lines in the data as well as shear and convergence signatures.

---

†This work was sponsored by the Federal Aviation Administration under Air Force Contract No. FA8721-05-C-0002. The views expressed are those of the authors and do not reflect the official policy or position of the U.S. Government. Opinions, interpretations, conclusions, and recommendations are those of the authors and are not necessarily endorsed by the US Government.

* *Corresponding author address*: David J. Smalley, MIT Lincoln Laboratory, 244 Wood Street, Lexington, MA 02420-9185. E-mail: daves@ll.mit.edu

TDWR and NEXRAD MIGFA versions; and some examples of MIGFA in operation.

2. MIGFA METHODOLOGY

MIGFA uses a multi-dimensional image processing approach to accrue evidence for the detection of gust fronts and other convergence phenomena. Input consists of radial velocity and reflectivity factor data remapped to Cartesian grids. The grids are viewed as 2D images that are analyzed by a technique called Functional Template Correlation yielding interest images (more details are provided later in this section). The gray-scale interest images depict, via pixel intensity, the likelihood of a particular piece of evidence, or feature, being present at that pixel location. The interest images are combined by pixel-wise weighted averaging into a single combined interest image from which MIGFA extracts the position of each gust front.

NEXRAD MIGFA uses radial velocity and reflectivity factor data from a combination of the 0.5^{o} and 1.5^{o} (1.3^{o} during VCP12 scanning) elevation angle tilts. The combination of lower tilts improves the data quality near the radar. The higher tilt is used within the first 20 km. This lessens the chance of interference from anomalous propagation (AP) and other clutter more often present on the lowest tilt. That lowest tilt is used beyond 25 km since the convergence phenomena that have operational significance to the FAA are surface based. The two tilts are linearly merged between 20 and 25 km.

MIGFA keys on three primary classes of signatures in the data imagery. Gust fronts and other convergence phenomena signatures typically appear in the data as thin lines. Figure 1 (upper panel) shows an example of such signatures in both the radial velocity and reflectivity factor data emanating from an area of convection to the southwest of the radar. The lower panel of Figure 1 depicts a different case with another class of feature signatures associated with the radial velocity data; namely, convergence signatures (denoted by arrows in the left image) and associated zones of radial shear. MIGFA maintains a history of these and other features through successive volumes, in part to determine the velocity of these features. Figure 2 illustrates the third class of signature: motion detection. The two leftmost images are reflectivity factor in successive volumes, and the rightmost image is the resultant difference that is used to determine feature motion.

The core technology of MIGFA is the use of knowledge-based image processing to examine the data for specific physical traits (signatures) relating to velocity convergence, thin lines, and motion. As noted, this is accomplished through functional template correlations (FTC) and interest images. The FTC consists of template-based pattern matching tailored to the signature of interest. This technique uses both the topology of the pattern in question and the pixel intensities to create an interest image. The pixel intensities in an interest image represent the strength of evidence, ranging from strongly against to strongly affirming.

MIGFA uses combinations of many interest images related to analysis of the individual surveillance and Doppler data fields. The schematic in Figure 3 illustrates the broad classes of features that generate the collection of interest images (i.e. - evidence) used. A single combined interest image results from averaging the individual interest images along with accounting for anticipation. From that, MIGFA extracts the detections (as a chain of points). Additionally, 10 and 20 minute forecast positions of these detection chains are determined.

3. "TUNING" MIGFA TO NEXRAD DATA

Each version of MIGFA is "tuned" to its input data source. The TDWR and NEXRAD radars have pencil beams, although the NEXRAD beam is near twice as wide as that for TDWR in this respect. NEXRAD also has coarser-grained range-bin resolution. The ASR-9 has two overlapping vertical fan beams. The differences in the subsequent data resolutions (particularly in the vertical) require thorough separate

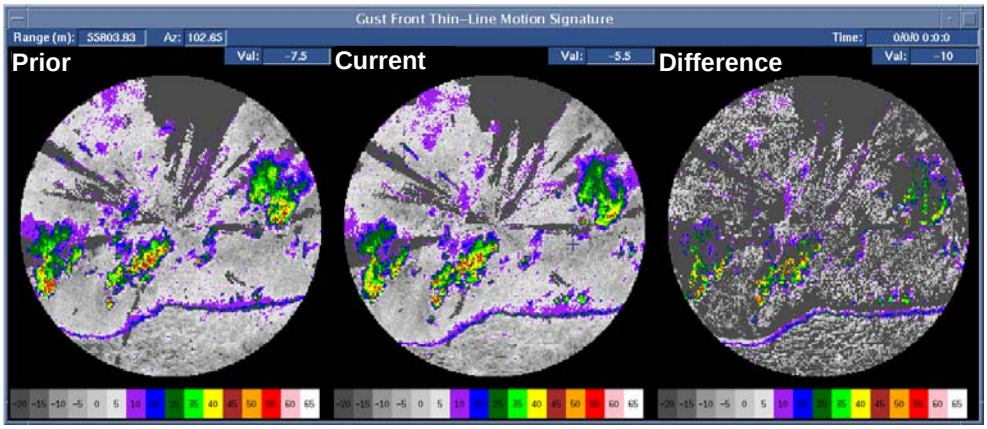

Figure 2. Motion, the difference in position of features in consecutive volumes, provides further interest fields for the MIGFA body of evidence.

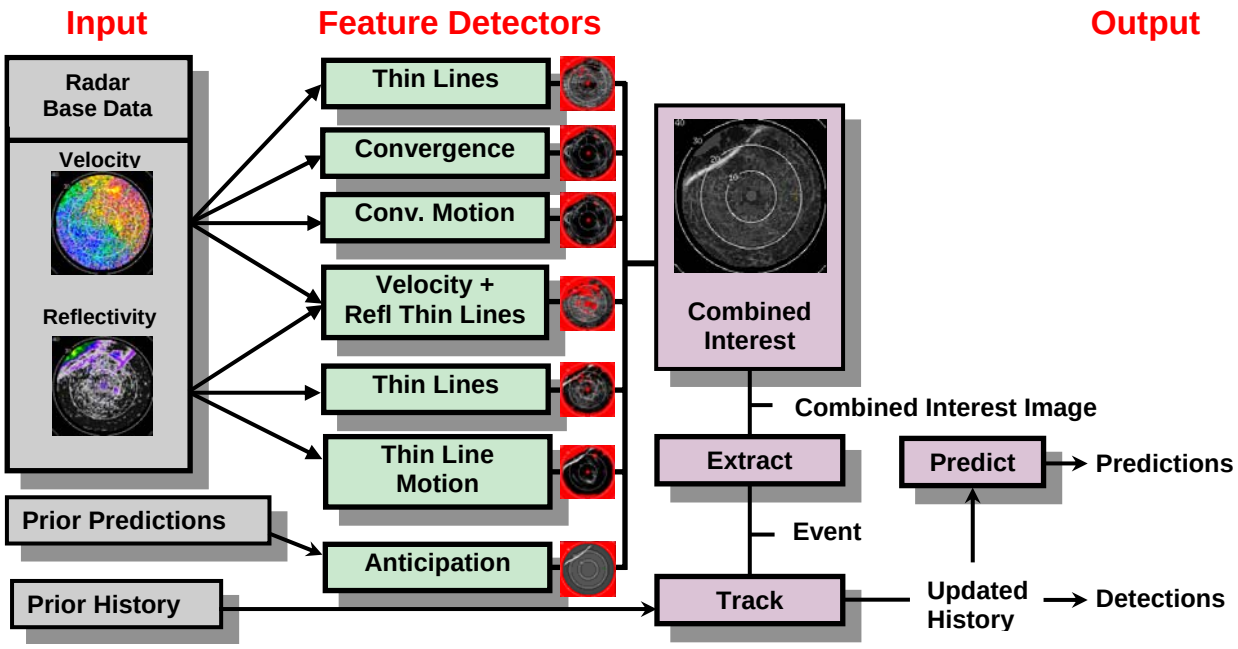

Figure 3. This schematic shows the general processing strategy of MIGFA. The input data consist of the lower tilt data from NEXRAD as well as related information from prior volumes. Many types of features are detected through knowledge-based image processing based on the three primary signatures of thin lines, convergence, and motion. The images are merged into a combined interest image from which detections and subsequent predictions and history are generated and updated.

analyses of MIGFA's performance to maximize the quality of the output product.

The analysis often entails assigning appropriate weights to those feature identifiers particularly sensitive to differing data resolutions. An extreme case of this is the ASR-9-based WSP Doppler velocity image that has high data variability caused by the vertical integration. This leads to low confidence in convergence feature detection for the WSP. Thus, the WSP convergence detectors receive relatively low weight compared to their TDWR and NEXRAD counterparts. This illustrates that relationships between the features and the radar beam characteristics sensing them are considered when tuning the performance parameters. By virtue of their pencil beams, those parameter values are very similar between the NEXRAD and TDWR MIGFA versions.

The tuning analysis yielded some differences between TDWR and NEXRAD MIGFA parameter values. Radar siting factors in these differences. TDWR sites were selected for their proximity to airports. Transient false alarms may be ignored in the case of TDWR MIGFA if they are a sufficient distance from the associated airport. Airport proximity received no special consideration regarding NEXRAD siting. With NEXRAD MIGFA intending to serve any airport in its domain, persistent sources of false alarms in the feature detectors needed to be mitigated Therefore, in NEXRAD MIGFA, reflectivity thin line detectors are slightly muted in comparison to their TDWR counterparts, because they tend to be a source of excessive false alarms.

In analyzing phenomena sensed by the different radars that lead to false alarm detections with MIGFA, it can happen that solutions extend beyond parameter tuning. For example, a significant source of false alarms for WSP was stratiform rain bands (observed as thin parallel banding) that can be mistaken by MIGFA for the leading edges of gust fronts. A technique was developed for mitigating this problem. In analyzing the performance of NEXRAD MIGFA, thin parallel banding signatures in non-precipitating conditions were noted as a source of false alarms. The stratiform-band-mitigation technology from WSP MIGFA was transferred to NEXRAD MIGFA. The resultant effect is that this type of false alarm has been nearly eliminated in NEXRAD MIGFA.

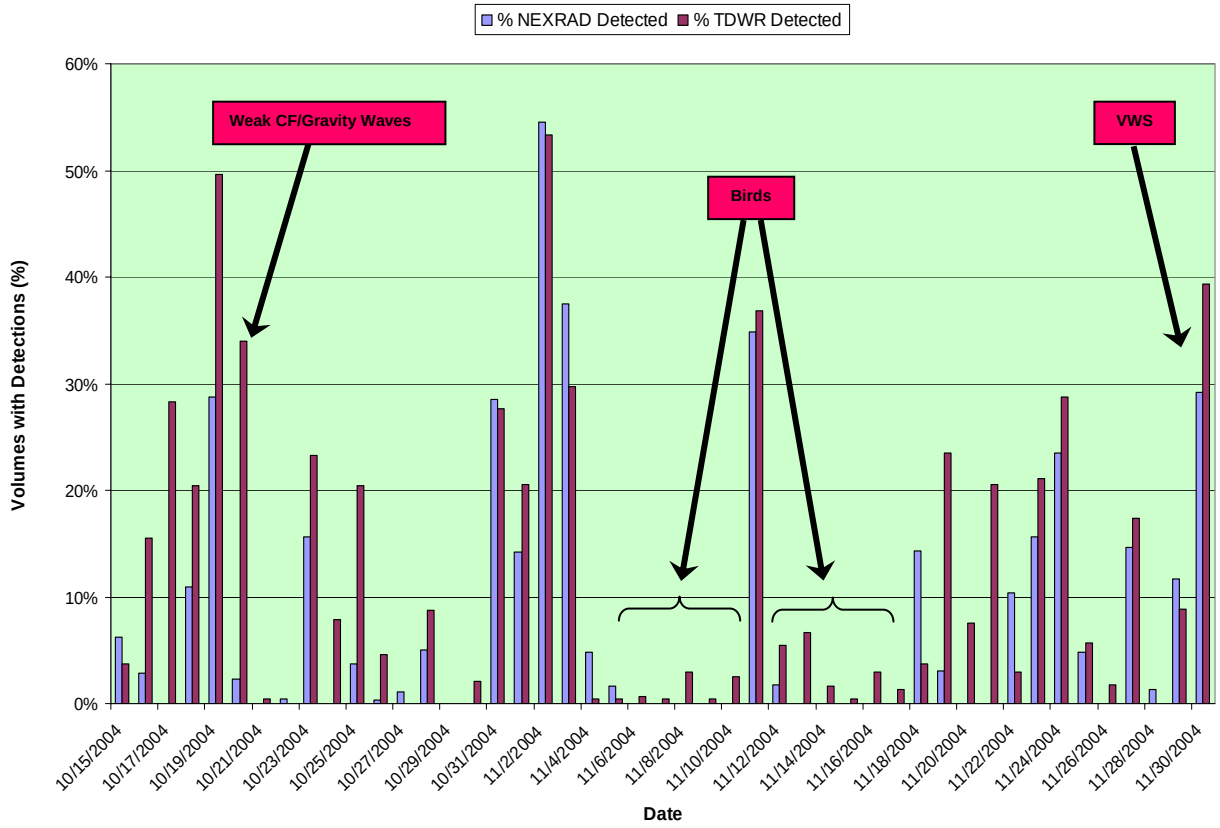

Figure 4. The chart shows the daily percentage of NEXRAD and TDWR radar volumes that their respective MIGFA versions yielded detections. The detections may be correct or false alarms. The data covers a 6 week period in October and November 2004 at Memphis, TN. The text discussion elaborates further on this and the versions' response to weak fronts, birds, and vertical wind shear (VWS).

4. MIGFA PERFORMANCE

NEXRAD MIGFA is intended to provide probability of detection performance as similar as possible to that which the FAA is accustomed to from the TDWR MIGFA. LL is monitoring the performance of NEXRAD MIGFA in a diverse set of locations in the U.S.: the coastal northeast, the east and west coasts of Florida, the southeast, the southern plains, and the southwest. The sites were partially selected due to either the TDWR or WSP versions of MIGFA being in operation nearby.

MIGFA typically performs somewhat differently in the "warm" season versus the more stressing "cool" season. The former is associated with convective weather while the latter covers the non-convective season. The primary contrast between the two seasons is essentially the much more favorable feature signal strength to background noise ratio during the warm season. The warm season poses the greatest hazard to aviation in terms of near surface wind shear, so it is fortuitous that the warm season signatures have better signal-to-noise ratios.

NEXRAD and TDWR MIGFA versions were compared for a six week period beginning in mid-October 2004 for the area near Memphis, TN. This is a cool season MIGFA study. Figure 4 shows the daily percentage of volumes with some sort of detections for the TDWR MIGFA (dark red) and NEXRAD MIGFA (blue). The radars do not have time synchronized radar volumes. The radars are also separated by about 40 km so do not have the same sampling volumes. Despite such differences, it was determined that there was a qualitatively acceptable similarity in responsiveness from the MIGFA versions during this study.

TDWR MIGFA is more sensitive under certain circumstances because of its finer resolution input data. Examples of such times are labeled in Figure 4 for conditions of weak cold fronts and gravity waves, and bird roost activity. It should be noted that NEXRAD MIGFA also could be stressed by biological signatures (birds and bats). In this circumstance, however, the TDWR MIGFA responded to bird roost activity because both the TDWR and bird roosts are located near the Memphis airport. Times of strong vertical wind shear (labeled VWS in Figure 4) lead to responses from both MIGFA versions.

The validity of the detections for this study was considered. Just as the two versions tracked well for the variety of weather conditions over the six week

SITE	SEASON	HOURS	STRENGTH	NEXRAD POD	NEXRAD PFA	TDWR POD	TDWR PFA
DFW	COOL	4	MEDIUM	90.9	16.7	100	25.0
DFW	COOL	3.5	STRONG	80.6	22.2	96.2	12.2
DFW	COOL	5	MEDIUM	95.3	15.2	91.2	24.0
DFW	COOL	3	STRONG	97.8	14.8	51.5	0.0
NQA	COOL	5	MEDIUM	74.6	17.5	81.3	2.6
NQA	COOL	3.5	MEDIUM	75.6	12.7	97.2	0.0
DFW	WARM	3	STRONG	43.4	0.0	79.5	2.9
DFW	WARM	3	STRONG	90.3	0.0	100	2.9
DFW	WARM	2	STRONG	95.7	0.0	100	15.4
DFW	WARM	4	MEDIUM	70.8	1.7	82.9	7.5
DFW	WARM	4	STRONG	67.6	4.2	91.5	8.1
DFW	WARM	3.5	MEDIUM	73.2	1.3	95.1	3.3
NQA	WARM	4	MEDIUM	74.7	5.2	66.7	2.2
NQA	WARM	3.5	MEDIUM	69.0	10.2	81.2	7.5
NQA	WARM	3	WEAK	55.0	0.0	85.7	1.9
TOTAL		**54**		**73.5**	**8.8**	**85.1**	**8.0**

Figure 5. Tabulation of NEXRAD and TDWR probability of detections (POD) and false alarms (PFA) for a mix of cases from Dallas-Fort Worth, TX (DFW) and Memphis, TN (NQA). The row shading indicates warm (tan) or cool (blue) season. The type is indicative of the dominant strength associated with the case: weak is 5-10 m s^{-1}; medium is 10-15 m s^{-1}; strong is 15-25 m s^{-1}. Section 4 includes further discussion.

period, the percentage of false alarm detections was similar. In this cool season analysis, the NEXRAD MIGFA had a false alarm rate of 31% compared with 27% for TDWR MIGFA.

A second study performed involved NEXRAD and TDWR MIGFA results from both Memphis, TN and Dallas-Fort Worth, TX. This data set includes more than 50 hours of truthed detection data. There are no cases that are entirely comprised of false alarms (i.e., all detections erroneous) in this set. The study is notable in that it includes warm and cool season cases; strong, medium, and weak wind shear cases; and wind shear variety from synoptic fronts to air mass convection.

Figure 5 lists the various cases comprising the set and the probability of detection (POD) and false alarm rates (PFA) for them individually and in total. It is evident that the cool season cases do have higher PFA than the warm season cases. Overall, the POD/PFA values for NEXRAD MIGFA (74/9) and TDWR MIGFA (85/8) for this study were similar.

A third study (not shown) was performed for NEXRAD MIGFA. This study did not compare performance results with corresponding TDWR MIGFA data. Over 200 hours worth of NEXRAD case data was truthed. The cases are from the TDWR-associated sites at Memphis, TN and Dallas-Fort Worth, TX and the WSP-associated sites at Austin, TX and Albuquerque, NM. The resultant POD was 70% with a 16% PFA. These results are similar to those from the study shown in Figure 5 for both versions. Consequently, MIGFA was accepted for Build 9 inclusion as a NEXRAD algorithm.

5. MIGFA EXAMPLES

In section 2, a general description was provided of some of the feature signatures that lead to MIGFA detections. There are multiple meteorological sources that can generate such signatures in the Planetary Boundary Layer. Two examples discussed here are supported by Figures 6 and 7. Those figures each have a sequence of five images. The images show the base reflectivity factor (left) and dealiased radial velocity (right) with MIGFA detections (solid yellow curves) and MIGFA 10 and 20 minute predictions (dashed yellow curves). The range ring intervals are 10 kilometers.

The Figure 6 case is from the KTBW (Tampa, FL) NEXRAD on May 16, 2005. This sequence of five images (A-E) depicts the evolution with time of two convectively induced gust fronts during a three hour interval. At the start (A), a number of relatively small but strong convective cells are noted generally southeast of the radar (center of the polar grid). No MIGFA detections appear at this time. Within 20 minutes, MIGFA has pieced together the incipient outflow boundary generated by the convection (B). During the following 50 minutes (C), the convection slowly drifts north and east continuing to support an outflow boundary. The relatively close spacing of the dashed prediction curves implies steady forward progress of the outflow. From the velocity data, an 8-12 m s^{-1} shear is observed with the outflow.

The southeastern portion of the outflow triggers convection over the next hour (D) that, in turn, produces its own outflow that MIGFA detects moving westward into the area southeast of the radar. The earlier

convection has vacated that area and continued to drift north and east with MIGFA still tracking its outflow boundary. Lastly (E), three hours from the sequence start (A), MIGFA is still detecting and tracking the boundaries. MIGFA's use of history and anticipation helps continue the tracking as signal density of the thin lines, convergence, and motion lessen.

Figure 7 is a case from the KEWX (New Braunfels, TX) NEXRAD on May 30, 2005. This sequence of five images (A-E) spans a two hour interval depicting an interesting interplay between weather and bats! The sequence begins (A) with convection to the southeast of the radar with MIGFA detecting an outflow boundary heading northwest. Over the course of the next hour (B), the convection maintains its strength and outflow as it drifts slightly north. MIGFA has greatly expanded the length of that outflow detection as it continues to progress northwestward. The portion east and north of the radar seems least supportable by the underlying data for this particular volume; but MIGFA's history and anticipation support the detection. This facet of MIGFA's processing is important especially at far distances from the radar where the radar beam is most elevated above the ground and most likely to be sensing weak signatures from shallow phenomena.

In addition, at this time (B), a boundary has been picked up to the north of the radar moving south and a reflectivity factor cell has popped up about 30 km west of the radar. Examination of the velocity data shows a divergence signature emanating from a point source. That return is actually the radar picking up the beginning of the mass exodus of millions of bats as they leave for dinner at dusk from Bracken Cave. As noted in National Geographic Magazine (McCracken and Westbrook, 2002), up to 20 million bats exit to feed at this time during the late spring. Their preferred feeding altitude ranges mainly to 3,200 feet placing them in prime view of the radar and prime altitude for MIGFA. In a mere 18 minutes (C), a very fast-growing radar echo covering over 300 km^2 has been generated by the bats! MIGFA has caught on to the outbound leading edge of this. Meanwhile, the outflow from the southeast continues to progress northwestward. In fact, its position (solid yellow curve) now (C) is as predicted (outer dashed yellow curve) 18 minutes earlier (B). MIGFA also still is tracking the boundary to the north where the convection has intensified.

During the next thirteen minutes (D), the bat area has quadrupled. The other two boundaries are still being tracked and MIGFA predictions (yellow dashed lines) signal some sort of bat-weather collision is coming. Note, though, that MIGFA has now dropped the northeastern-most portion of the long boundary from the southeast convection. The convection north of the radar continues to remain strong. Within the half hour (E), the boundaries have met in some areas. Notably, the original boundary (A) from the southeast convection has intersected with the convection (and boundary) north of the radar. At that juncture, the convection is most intense. While the original boundary did not cause convective initiation there, it likely has enhanced it at this time.

6. SUMMARY

MIGFA was developed by LL as a response to an established need of the FAA to detect and predict the locations of wind shear hazards impacting airports. NEXRAD MIGFA is the third in a series of MIGFAs developed over the past decade designed to detect such hazards in data from FAA weather radars. The three versions share the same core image processing techniques. Any further capabilities added to one version of MIGFA could easily be shared with the other versions as appropriate. NEXRAD MIGFA has been tuned to provide results similar to that of the TDWR MIGFA.

MIGFA provides information of interest to aviation and non-aviation users. Both the NWS and DoD plan to use it in their weather systems. The two examples illustrate the capability that the MIGFA product brings to NEXRAD. For purposes here, the examples were kept relatively simple and legible. However, during testing and evaluation of NEXRAD MIGFA, many complex multiple boundary interactions were observed that were best served by the automated detection and prediction from MIGFA.

7. ACKNOWLEDGEMENT

This algorithm development is sponsored by the FAA. MIGFA has a long history of development on multiple radar platforms at LL. Many current and former colleagues of MIT Lincoln Laboratory's Weather Sensing Group have contributed. Those contributing to this specific version include John Morgan, Justin Shaw, Beth Echels, Erik Proseus, and Mark Isaminger. Their efforts are much appreciated.

8. REFERENCES

Delanoy, R.L. and S.W. Troxel, 1993: The Machine Intelligent Gust Front Algorithm. MIT Lincoln Laboratory Project Report ATC-196.

McCracken, G.F. and J.K. Westbrook, 2002: "Bat Patrol", *National Geographic Magazine*.

Morgan, J. and S. Troxel, 2002: CSKETCH Image Processing Library. MIT Lincoln Laboratory Project Report ATC-283.

Smalley, D.J., B.J. Bennett, and M.L. Pawlak, 2003: New Products for the NEXRAD ORPG to Support FAA Critical Systems. 19th International Conference on Interactive Information Processing Systems (IIPS) for Meteorology, Hydrology, and Oceanography, Long Beach, CA, Amer. Meteor. Soc., paper 14.12.

Troxel, S.W. and W.L. Pughe, 2002: Machine Intelligent Gust Front Algorithm for the WSP. MIT Lincoln Laboratory Project Report ATC-274.

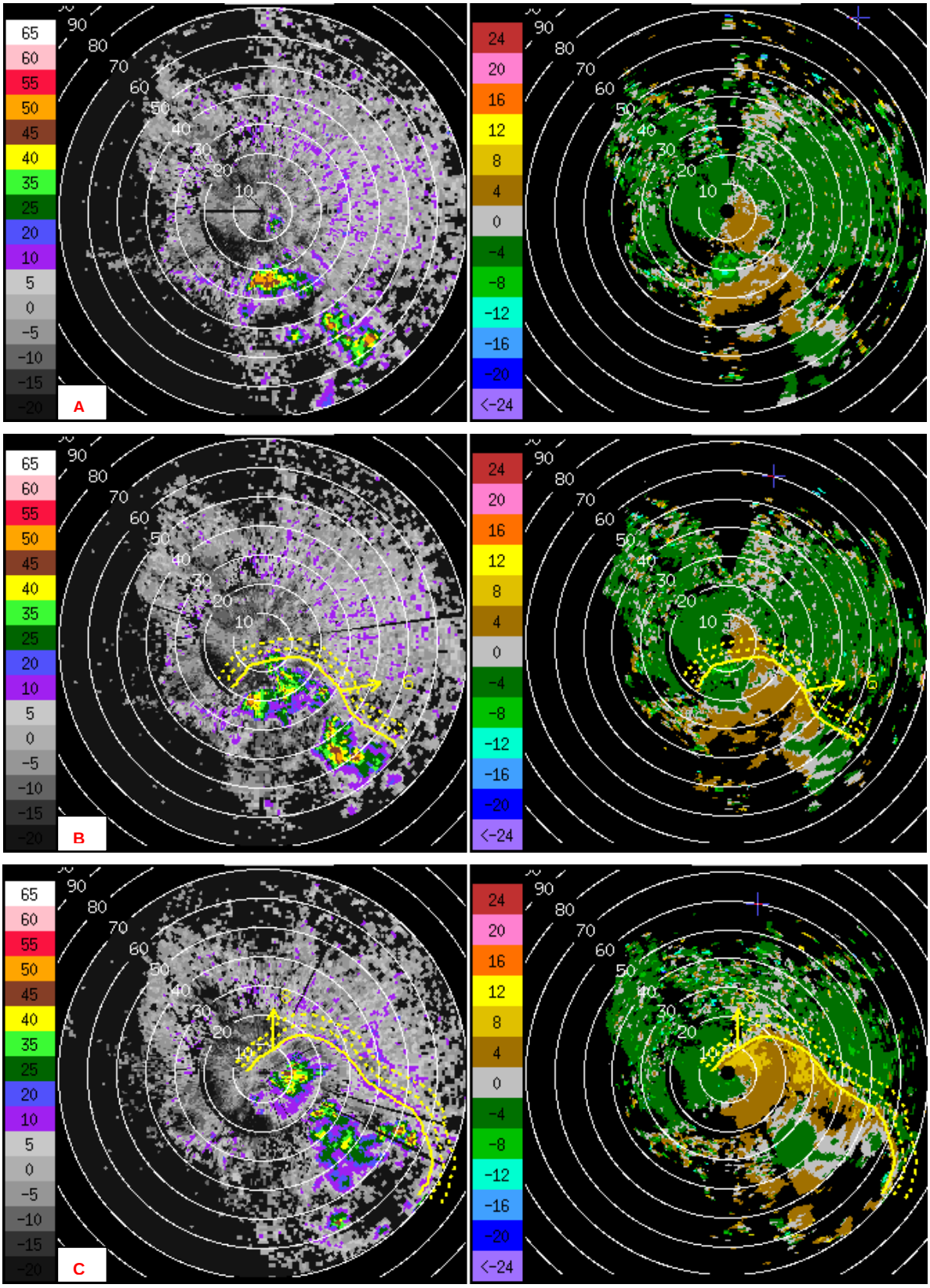

Figure 6. This is a sequence of radar reflectivity factor (left) and dealiased radial velocity (right) images with NEXRAD MIGFA detections (yellow solid and dashed curves) from the Tampa Bay, FL NEXRAD (KTBW) from May 16, 2005 for UTC times 20:19 (A), 20:40 (B), and 21:31 (C). Refer to the text for a discussion.

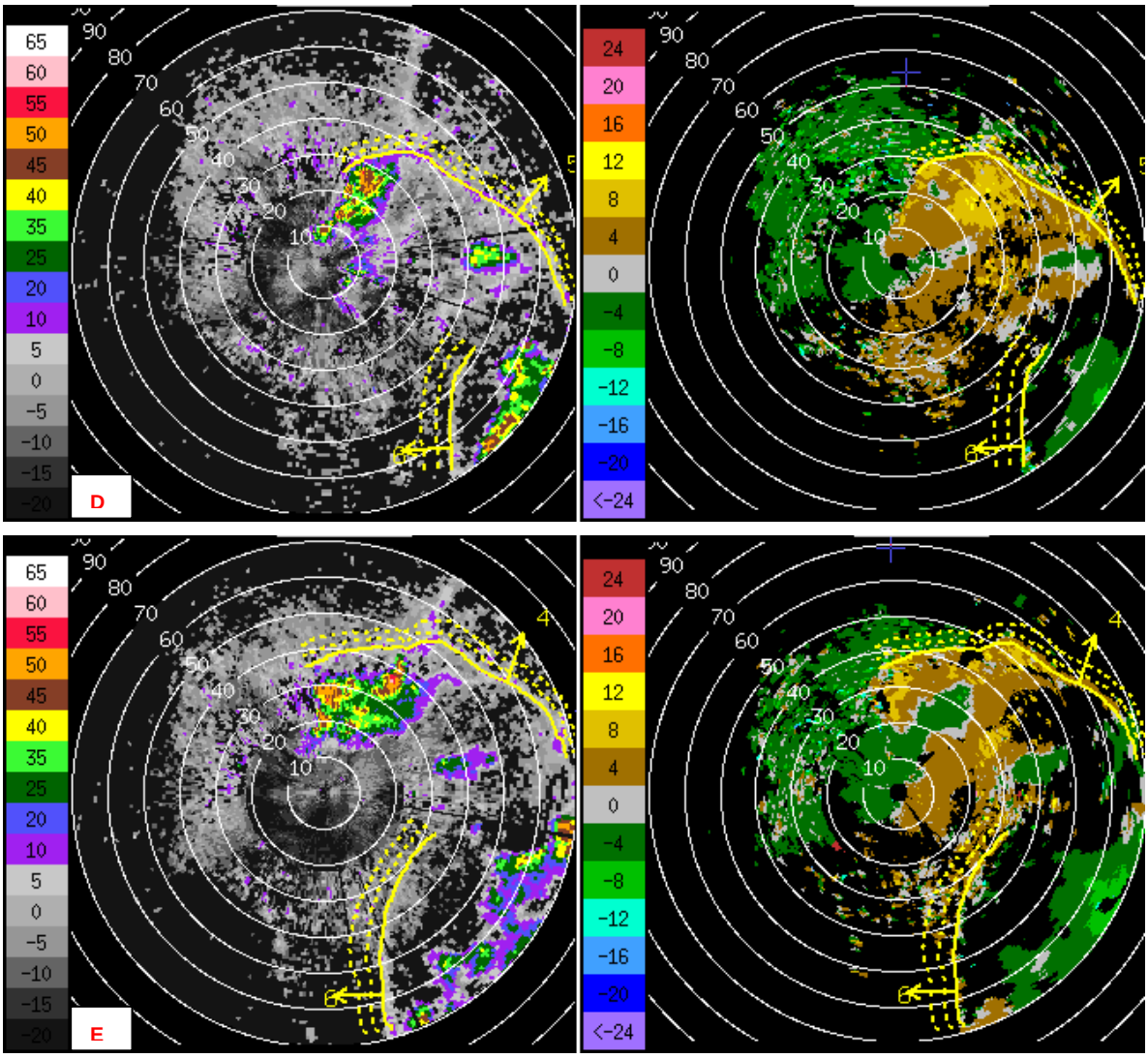

Figure 6 (cont.). This is a sequence of radar reflectivity factor (left) and dealiased radial velocity (right) images with NEXRAD MIGFA detections (yellow solid and dashed curves) from the Tampa Bay, FL NEXRAD (KTBW) from May 16, 2005 for UTC times 22:33 (D) and 23:19 (E). Refer to the text for a discussion.

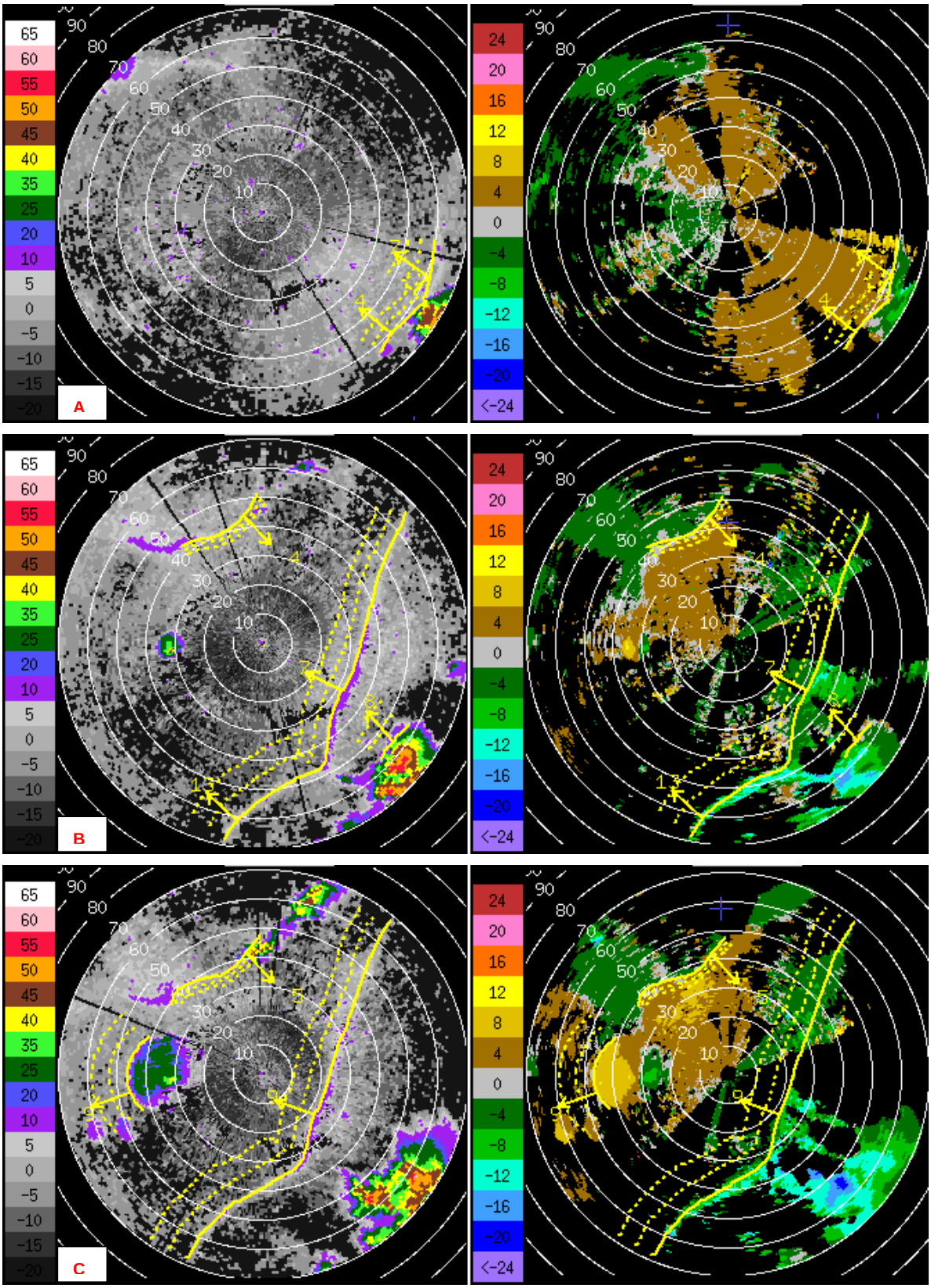

Figure 7. This is a sequence of radar reflectivity factor (left) and dealiased radial velocity (right) images with NEXRAD MIGFA detections (yellow solid and dashed curves) from the New Braunfels, TX NEXRAD (KEWX) from May 30, 2005 for UTC times 00:03 (A), 01:03 (B), and 01:21 (C). Refer to the text for a discussion.

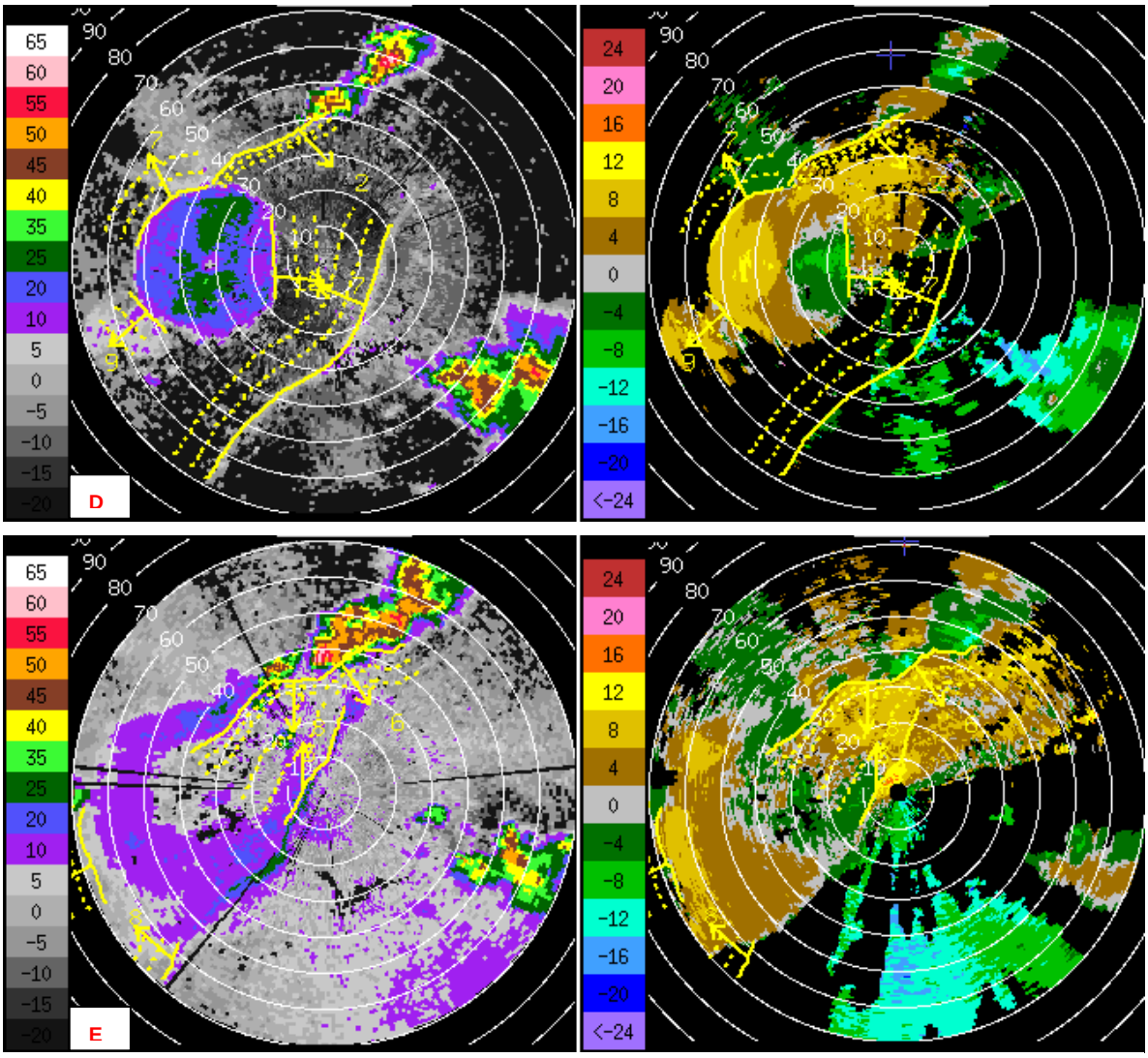

Figure 7 (cont.). This is a sequence of radar reflectivity factor (left) and dealiased radial velocity (right) images with NEXRAD MIGFA detections (yellow solid and dashed curves) from the New Braunfels, TX NEXRAD (KEWX) from May 30, 2005 for UTC times 01:34 (D) and 02:04 (E). Refer to the text for a discussion.